Engineering Analysis with Boundary Elements 83 (2017) 195–203

Contents lists available at ScienceDirect

Engineering Analysis with Boundary Elements

journal homepage: www.elsevier.com/locate/enganabound

Micro-structured materials: Inhomogeneities and imperfect interfaces in plane micropolar elasticity, a boundary element approach

Elena Atroshchenko[a,*], Jack S. Hale[b], Javier A. Videla[a], Stanislav Potapenko[c], Stéphane P.A. Bordas[b,d,e]

[a] Department of Mechanical Engineering, University of Chile, Santiago 8370448, Chile
[b] Institute for Computational Engineering, Faculty of Science, Technology and Communication, University of Luxembourg, Luxembourg
[c] Department of Civil and Environmental Engineering, University of Waterloo, ON, Canada
[d] Cardiff University, Institute of Mechanics and Advanced Materials, School of Engineering, College of Physical Sciences and Engineering, UK
[e] University of Western Australia, Intelligent Systems for Medicine Laboratory, School of Mechanical and Chemical Engineering, Australia

ARTICLE INFO

Keywords:
Cosserat elasticity
Boundary integral equation method
Inclusion
FEniCS

ABSTRACT

In this paper we tackle the simulation of microstructured materials modelled as heterogeneous Cosserat media with both perfect and imperfect interfaces. We formulate a boundary value problem for an inclusion of one plane strain micropolar phase into another micropolar phase and reduce the problem to a system of boundary integral equations, which is subsequently solved by the boundary element method. The inclusion interface condition is assumed to be imperfect, which permits jumps in both displacements/microrotations and tractions/couple tractions, as well as a linear dependence of jumps in displacements/microrotations on continuous across the interface tractions/couple traction (model known in elasticity as *homogeneously imperfect interface*). These features can be directly incorporated into the boundary element formulation.

The BEM-results for a circular inclusion in an infinite plate are shown to be in an excellent agreement with the analytical solutions. The BEM-results for inclusions in finite plates are compared with the FEM-results obtained with FEniCS.

1. Introduction

This paper presents the first application and verification of the boundary element method to simulate the mechanical effects of inclusions with imperfect interfaces in plane micropolar elasticity.

Modern nano-technological applications such as sensors and actuators, microelecromechanical systems, electronic packaging, advanced nano-composites call for efficient approaches to model the mechanical behavior of micro and nano-structured materials. Atomistic simulations are one way forward, but these are extremely computationally expensive[1], such that multi-scale approaches are required e.g. see [2]. One approach to account for the multi-scale nature of materials is to build continuum scale constitutive theories able to reproduce the continuum behavior of such nano/micro-structured materials, see e.g. [3] for an account of continuum models of micro-structured materials. The micropolar theory is one such approach, which we use in this paper.

Micropolar (also known as Cosserat) elasticity was first introduced by the Cosserat brothers [4] and further developed by Eringen [5], Nowacki [6], Eremeyev [7] etc., and it is able to account for the rotation of individual material points (differential elements). This leads to the description of a deformed state in terms of asymmetric stress and couple stress tensors. It was shown that micropolar constitutive models, in spite of being a continuum model, are able to replicate the experimentally-observed behavior of natural or engineered materials possessing micro or nano structures [3] such as bone [8–11], fibre-reinforced composites [12–14], blocky and layered materials, such as rock and rock masses [15–17], cellular materials [18,19] and many others.

The problem of (imperfect) interfaces (also known as interphases) in Cosserat matter was scarcely addressed [20], whilst it was much more intensively modelled and simulated in the context of standard linear elasticity, with or without surface effects, see e.g. [21–26] for implementation aspects. It is however interesting to note that Cosserat materials have been themselves used to model the mechanical effects of such interphases within heterogeneous materials, as discussed in depth in recent literature [27,28].

* Corresponding author.
E-mail address: eatroshchenko@ing.uchile.cl (E. Atroshchenko).

[1] Some estimates claim that it will be 80 years before the failure of one cubic centimeter of metal can be simulated using such approaches [1].

http://dx.doi.org/10.1016/j.enganabound.2017.07.023
Received 28 October 2016; Received in revised form 14 July 2017; Accepted 20 July 2017
Available online 17 August 2017
0955-7997/

Due to the rapid development of composite materials for advanced engineering applications, the problem of quantifying the effects of heterogeneities is crucially important, in particular in cases where the interfaces between the bulk/matrix and the inclusions are imperfect or carry surface energy.

The effects of heterogeneities/inhomogeneities have been studied well within the confines of Cauchy continua (classical elasticity), both analytically and numerically, starting from the classical Muskhelishvili's problem of a circular inclusion in an infinite plate [29] to the finite and boundary element analysis of multiple inclusions of various shapes, see for example [30–32] and crack/inclusion interactions, e.g. [33] and more recently [34].

In Cosserat elasticity, however, less work has been done and much remains to be understood about Cosserat-heterogeneous materials. Such efforts date back to 1976 with the work of [35]. In the 1990s significant work has been done on Cosserat-heterogeneous materials to study the effects of inclusions [36] and compute homogenized properties and their bounds and to understand their asymptotic behavior [37–39]. An interesting result of [39] is that if ℓ is the size of the Cosserat-heterogeneities, ℓ_c the Cosserat intrinsic length scales and L the size of the material sample, $\ell \approx \ell_c \ll L$ leads to a Cauchy continuum, whereas if $\ell_c \approx L$ then, the effective (homogenized) medium is better approximated by a Cosserat material.

More recently, work on Cosserat-heterogeneous materials has intensified somewhat with the work of [40], who provides analytical solutions in plane strain and [27,28] who focus on the modelling of interphases in heterogeneous materials by a non-linear Cosserat material.

A number of analytical and numerical methods have been developed to treat boundary value problems of micropolar elasticity. The finite element method remains the most common tool of numerical analysis [41–45].

Recently, the boundary element method [46] and [47] has been emerging as a powerful alternative due to its advantage in treating problems with non-smooth boundaries and infinite domains. For example, in [46] the dual boundary element method was applied to crack problems in plane strain micropolar continua.

One of the advantages of using boundary elements for inclusion problems, is the ability to incorporate the model of imperfect interfaces directly into the boundary integral formulation, keeping the linear formulation of the problem, while in the case of finite element method such interface model would make the formulation nonlinear. In this work we use the simple imperfect interface model, known as *homogeneously imperfect interface*, which is characterised by tractions and couple traction being continuous across the interface, and proportional to the jumps in displacements and out-of-plane microrotation. This model, for a circular inclusion in a plate subjected to uni-axial tension was investigated analytically in [48] with the full solution available in [49].

Another imperfect interface model, used in this work, is characterized by arbitrary jumps in both surface tractions/couple traction, as well as in displacements and out-of-plane microration. Physically, such a model allows to impose more general boundary conditions, while mathematically it brings additional advantages for the problems in infinite domain, because it enables to significantly reduce the size of the problem by transferring the boundary conditions at infinity to the boundary conditions on the inclusion interface.

In this paper we develop a system of boundary integral equations for an inclusion problem in plane micropolar and solve it by the boundary element method. We show the excellent agreement of the BEM-results with the analytical and FEM-solutions. We present the BEM-study of micropolar effects on inclusions of various shapes under various loading conditions. We demonstrate the dependence of the stress concentration factors on material parameters, including the limiting cases, when one material is nearly classical, while the second one is strongly micropolar. These parametric studies give a deeper insight into the mechanics of micropolar inhomogeneities. The developed solutions can also serve as benchmark problems for further use with other analytical and numerical methods.

The paper is organized as follows. In chapter 2 we formulate the boundary value problem of an inclusion in micropolar plane strain. In chapter 3 we derive the system of boundary integral equations. In chapter 4 we briefly outline the boundary element method procedure. Numerical results are given in chapter 5, while chapter 6 contains discussion of the results and directions of future work.

2. Mathematical formulation of an inclusion problem

According to [5], a plane strain deformation of a micropolar material is described by two in-plane displacements $u_1 = u_1(\boldsymbol{x})$, $u_2 = u_2(\boldsymbol{x})$ and one out-of-plane microrotation $\phi_3 = \phi_3(\boldsymbol{x})$, where $\boldsymbol{x} = (x_1, x_2)$, which we combine into one vector of generalized displacements: $\boldsymbol{u} = (u_1, u_2, u_3)^T$ with $u_3 = \phi_3$. In absence of body forces and couples, the equations of equilibrium for a material described by parameters λ, μ, κ and γ can be written as

$$L(\partial_x)\boldsymbol{u} = 0, \tag{1}$$

where the matrix differential operator $L(\partial_x) = L(\xi_\alpha)$ is given in [50], [51] as

$$L(\xi_\alpha) = \begin{pmatrix} (\lambda+\mu)\xi_1^2 + (\mu+\kappa)\Delta & (\lambda+\mu)\xi_1\xi_2 & \kappa\xi_2 \\ (\lambda+\mu)\xi_1\xi_2 & (\lambda+\mu)\xi_2^2 + (\mu+\kappa)\Delta & -\kappa\xi_1 \\ -\kappa\xi_2 & \kappa\xi_1 & \gamma\Delta - 2\kappa \end{pmatrix}, \tag{2}$$

with $\xi_\alpha = \partial/\partial x_\alpha$ and $\Delta = \partial^2/\partial x_1^2 + \partial^2/\partial x_2^2 = \xi_1^2 + \xi_2^2$.

Two tractions $t_1 = t_1(\boldsymbol{x})$, $t_2 = t_2(\boldsymbol{x})$ and one couple-traction $t_3 = t_3(\boldsymbol{x})$, defined on a boundary with normal $\boldsymbol{n} = (n_1, n_2)^T$, are also combined into vector $\boldsymbol{t} = (t_1, t_2, t_3)^T$. By the standard definition

$$t_\alpha = \sigma_{\beta\alpha} n_\beta, \quad t_3 = m_{\beta 3} n_\beta, \quad \alpha, \beta = 1, 2. \tag{3}$$

where σ_{11}, σ_{12}, σ_{21}, σ_{22} are components of the asymmetric micropolar stress tensor and m_{13}, m_{23} are the couple-stresses.

Together with $L(\xi_\alpha)$ the boundary stress operator $T(\partial_x) = T(\xi_\alpha)$ is considered [50], which is defined by the following equation:

$$T(\xi_\alpha) = \begin{pmatrix} (\lambda+2\mu+\kappa)\xi_1 n_1 + (\kappa+\mu)\xi_2 n_2 & \lambda\xi_2 n_1 + \mu\xi_1 n_2 & \kappa n_2 \\ \mu\xi_2 n_1 + \lambda\xi_1 n_2 & (\mu+\kappa)\xi_1 n_1 + (\lambda+2\mu+\kappa)\xi_2 n_2 & -\kappa n_1 \\ 0 & 0 & \gamma\xi_\alpha n_\alpha \end{pmatrix} \tag{4}$$

Operator $T(\partial_x)$ is defined according to the stress strain relations and the constitutive equations, as given in [5] in such a way that

$$\boldsymbol{t} = T(\partial_x)\boldsymbol{u}. \tag{5}$$

Together with constants λ, μ, γ, κ, we use engineering constants: G (shear modulus), ν (Poisson's ratio), ℓ (characteristic length) and N (coupling number), defined in [8].

We consider a bounded inclusion occupying the domain S^i with the boundary ∂S^i and inner normal $\vec{n}$ as shown in Fig. 1. The inclusion is made of homogeneous and isotropic micropolar material with elastic constants λ^i, μ^i, κ^i, γ^i. The matrix, which occupies domain S^e is also homogeneous and isotropic micropolar material with elastic constants λ^e, μ^e, κ^e, γ^e. The engineering material parameters, describing the inclusion or the matrix are denoted as G^i, ν^i, ℓ^i, N^i or G^e, ν^e, ℓ^e, N^e respectively.

Let $L^i(\partial_x)$ and $L^e(\partial_x)$ be the operator $L(\partial_x)$ with constants λ^i, μ^i, κ^i, γ^i and λ^e, μ^e, κ^e, γ^e respectively. The boundary stress operators $T^i(\partial_x)$ and $T^e(\partial_x)$ are defined analogously. The displacement vector in domain S^i is denoted as $\boldsymbol{u}^i$, in domain S^e as $\boldsymbol{u}^e$. The boundary tractions are defined as

$$\boldsymbol{t}^i = T^i(\partial_x)\boldsymbol{u}^i, \quad \boldsymbol{t}^e = T^e(\partial_x)\boldsymbol{u}^e. \tag{6}$$

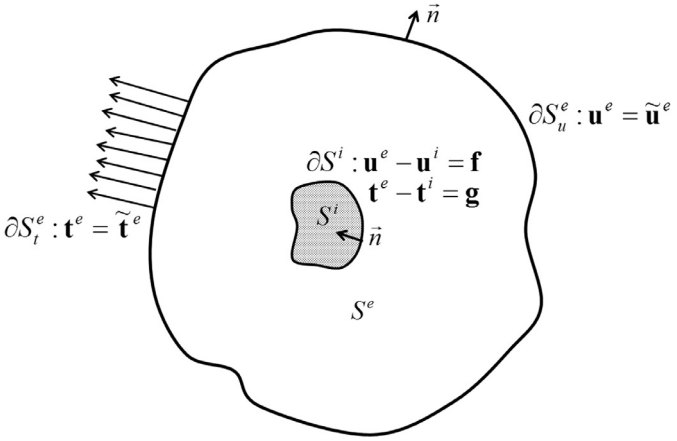

Fig. 1. Inclusion boundary value problem given by Eq. (7).

The first boundary value problem for an inclusion with the imperfect interface, that we consider in this paper, is given as follows:

$$\begin{aligned} L^i(\partial_x)\boldsymbol{u}^i &= 0 \text{ in } S^i,\\ L^e(\partial_x)\boldsymbol{u}^e &= 0 \text{ in } S^e,\\ \boldsymbol{u}^e &= \tilde{\boldsymbol{u}}^e \text{ on } \partial S_u^e,\\ \boldsymbol{t}^e &= \tilde{\boldsymbol{t}}^e \text{ on } \partial S_t^e,\\ \boldsymbol{u}^e - \boldsymbol{u}^i &= \boldsymbol{f} \text{ on } \partial S^i,\\ \boldsymbol{t}^e - \boldsymbol{t}^i &= \boldsymbol{g} \text{ on } \partial S^i, \end{aligned} \tag{7}$$

where $\tilde{\boldsymbol{u}}$ is the generalized displacement vector, consisting of two displacements and one microrotation prescribed on Dirichlet part ∂S_u^e of the outer boundary ∂S^e and vector $\tilde{\boldsymbol{t}}$ is the generalized traction vector, consisting of two tractions and one couple traction prescribed on Neumann part ∂S_t^e of ∂S^e. Jump in displacements and micro-rotation along the inclusion interface is described by function $\boldsymbol{f} = (f_1, f_2, f_3)^T$, while jump in tractions and couple tractions is given by $\boldsymbol{g} = (g_1, g_2, g_3)^T$. A perfect interface is characterized by $\boldsymbol{f} = \{0,0,0\}$ and $\boldsymbol{g} = \{0,0,0\}$.

Together with the interface boundary conditions given by the last two equations of Eq. (7) we consider the case of so-called homogeneously imperfect interface characterized by continuous stresses and jumps in the normal and tangential displacements proportional to the corresponding stress components. In micropolar elasticity two additional conditions need to be imposed, namely, continuous couple traction and jump in the microrotations proportional to the couple traction [48]. These conditions are written as:

$$\begin{aligned} \sigma_{nn}^e &= \sigma_{nn}^i,\\ \sigma_{nt}^e &= \sigma_{nt}^i,\\ m_{nz}^e &= m_{nz}^i,\\ u_n^e - u_n^i &= \lambda_n \sigma_{nn}^e,\\ u_t^e - u_t^i &= \lambda_t \sigma_{nt}^e,\\ \phi^e - \phi^i &= \lambda_\phi m_{nz}^e, \end{aligned} \tag{8}$$

where λ_n, λ_t, λ_z are the interface parameters [48]. The firstenlrg three equations are equivalent to the condition $\boldsymbol{t}^e = \boldsymbol{t}^i$, while the last three equations we rewrite as

$$\boldsymbol{u}^e - \boldsymbol{u}^i = \boldsymbol{A}(\boldsymbol{x})\,\boldsymbol{t}^e, \tag{9}$$

where

$$\boldsymbol{A}(\boldsymbol{x}) = \begin{pmatrix} n_1^2\lambda_n + n_2^2\lambda_t & n_1 n_2(\lambda_n - \lambda_t) & 0\\ n_1 n_2(\lambda_n - \lambda_t) & n_2^2\lambda_n + n_1^2\lambda_t & 0\\ 0 & 0 & \lambda_\phi \end{pmatrix}. \tag{10}$$

Therefore, the second boundary value problem that we consider in this paper is written as

$$\begin{aligned} L^i(\partial_x)\boldsymbol{u}^i &= 0 \text{ in } S^i,\\ L^e(\partial_x)\boldsymbol{u}^e &= 0 \text{ in } S^e,\\ \boldsymbol{u}^e &= \tilde{\boldsymbol{u}}^e \text{ on } \partial S_u^e,\\ \boldsymbol{t}^e &= \tilde{\boldsymbol{t}}^e \text{ on } \partial S_t^e,\\ \boldsymbol{u}^e - \boldsymbol{u}^i &= \boldsymbol{A}(\boldsymbol{x})\,\boldsymbol{t}^e \text{ on } \partial S^i,\\ \boldsymbol{t}^e &= \boldsymbol{t}^i \text{ on } \partial S^i. \end{aligned} \tag{11}$$

3. Boundary integral equations.

The boundary integral equations of plane Cosserat elasticity for an arbitrary domain S with boundary ∂S and outward normal $\vec{n}$ are formulated as follows:

$$\frac{1}{2}u_i(\boldsymbol{x}) + \fint_{\partial S} P_{ij}(\boldsymbol{x},\boldsymbol{y})u_j(\boldsymbol{y})ds_y - \int_{\partial S} D_{ij}(\boldsymbol{x},\boldsymbol{y})t_j(\boldsymbol{y})ds_y = 0, \quad i,j = 1,2,3. \tag{12}$$

where $\boldsymbol{x} \in \partial S$ is called a source point, $\boldsymbol{y} \in \partial S$ is a field point. Matrices of fundamental solutions $D_{ij}(\boldsymbol{x},\boldsymbol{y})$, $P_{ij}(\boldsymbol{x},\boldsymbol{y})$ are given in [52]. According to their asymptotic behavior in the vicinity of $\boldsymbol{x} = \boldsymbol{y}$, which explained in details in [46], components D_{11}, D_{22}, D_{33} have logarithmic singularity, while P_{12} and P_{21} are singular and the corresponding integrals are understood in the sense of Cauchy Principal Value, as indicated by sign $\fint$.

In what follows $D_{ij}^i(\boldsymbol{x},\boldsymbol{y})$, $P_{ij}^i(\boldsymbol{x},\boldsymbol{y})$ denote matrices of fundamental solutions corresponding to the inclusion, described by material parameters with superscript i, while $D_{ij}^e(\boldsymbol{x},\boldsymbol{y})$, $P_{ij}^e(\boldsymbol{x},\boldsymbol{y})$ correspond to domain S^e. Eq. (12) can be directly prescribed for domain S^e as

$$\frac{1}{2}u_i^e(\boldsymbol{x}) + \fint_{\partial S^e \bigcup \partial S^i} P_{ij}^e(\boldsymbol{x},\boldsymbol{y})u_j^e(\boldsymbol{y})ds_y - \int_{\partial S^e \bigcup \partial S^i} D_{ij}^e(\boldsymbol{x},\boldsymbol{y})t_j^e(\boldsymbol{y})ds_y = 0 \tag{13}$$

For domain S^i due to the inward orientation of the normal, the equation reads as follows:

$$\frac{1}{2}u_i^i(\boldsymbol{x}) - \fint_{\partial S^i} P_{ij}^i(\boldsymbol{x},\boldsymbol{y})u_j^i(\boldsymbol{y})ds_y + \int_{\partial S^i} D_{ij}^i(\boldsymbol{x},\boldsymbol{y})t_j^i(\boldsymbol{y})ds_y = 0 \tag{14}$$

Applying the jump boundary conditions of Eq. (7), Eq. (14) can be rewritten as:

$$\frac{1}{2}u_i^e(\boldsymbol{x}) - \fint_{\partial S^i} P_{ij}^i(\boldsymbol{x},\boldsymbol{y})u_j^e(\boldsymbol{y})ds_y + \int_{\partial S^i} D_{ij}^i(\boldsymbol{x},\boldsymbol{y})t_j^e(\boldsymbol{y})ds_y = p_i(\boldsymbol{x}), \tag{15}$$

where

$$p_i(\boldsymbol{x}) = \frac{1}{2}f_i(\boldsymbol{x}) - \fint_{\partial S^i} P_{ij}^i(\boldsymbol{x},\boldsymbol{y})f_j(\boldsymbol{y})ds_y + \int_{\partial S^i} D_{ij}^i(\boldsymbol{x},\boldsymbol{y})g_j(\boldsymbol{y})ds_y. \tag{16}$$

If boundary conditions of Eq. (11) are used instead of Eq. (7), then Eq. (14) becomes

$$\frac{1}{2}u_i^e(\boldsymbol{x}) - \fint_{\partial S^i} P_{ij}^i(\boldsymbol{x},\boldsymbol{y})u_j^e(\boldsymbol{y})ds_y + \int_{\partial S^i} D_{ij}^i(\boldsymbol{x},\boldsymbol{y})t_j^e(\boldsymbol{y})ds_y - \frac{1}{2}A_{ij}(\boldsymbol{x})t_j(\boldsymbol{x}) + \fint_{\partial S^i} P_{ik}^i(\boldsymbol{x},\boldsymbol{y})A_{kj}(\boldsymbol{y})t_j^e(\boldsymbol{y})ds_y = 0. \tag{17}$$

Then the full system of boundary integral equations for the inclusion problem is given by Eq. (13) + Eq. (15) or Eq. (13) + Eq. (17), where $u^e(\boldsymbol{x})$ and $t^e(\boldsymbol{x})$ are both unknown along the entire inclusion interface ∂S^i, while on the outer boundary ∂S^e the equations are solved for $u^e(\boldsymbol{x})$ on ∂S_t^e and for $t^e(\boldsymbol{x})$ on ∂S_u^e.

For the discretization of these BIEs we use a classical approach with quadratic Lagrange basis functions. For the evaluation of all weakly-singular integrals Telles transform [53] is used, while the singular integrals are evaluated using the singularity subtraction technique (SST), based on the asymptotic expansions of the matrices of fundamental solutions, given in [46]. After the values of displacements/microrotation

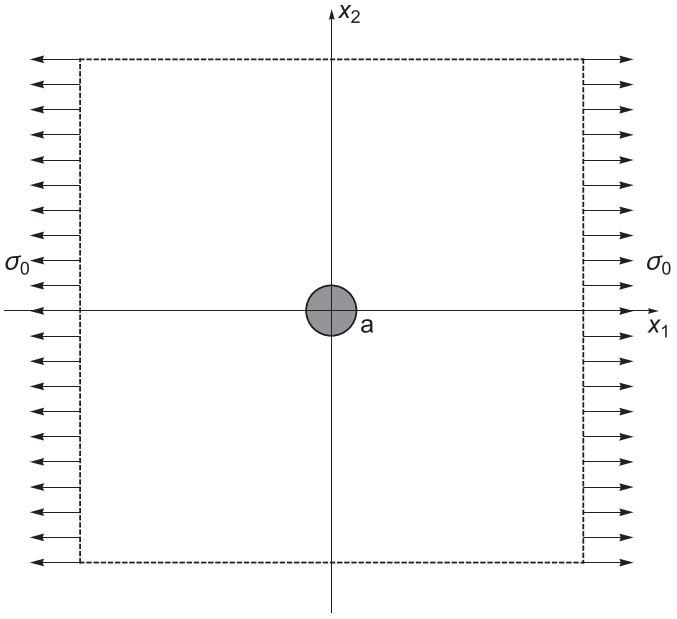

Fig. 2. Circular inclusion in an infinite plate under remote tension.

and tractions/couple tractions are evaluated along the boundary, the values of $\boldsymbol{u}^i$, $\boldsymbol{u}^e$ and $\boldsymbol{t}^i$, $\boldsymbol{t}^e$ inside the inclusion domain S^i and the matrix domain S^e respectively can be calculated using the micropolar analogues of Somiglina's displacement and stress identities, described in [46]. The expressions for two more matrices of fundamental solutions, used in Somiglina's representation of the stresses and couple stresses inside a domain, are provided in a ready-to-use form in [52].

4. Numerical results

4.1. Example 1. Circular inclusion in an infinite domain under remote tension: perfect interface.

In the first example we consider an infinite plate subjected to the uniform tension and containing a circular inclusion of radius a with perfect interface, as shown in Fig. 2. To take the full advantage of the boundary element method for problems with infinite domains, we seek the solution of this problem as a superposition of two solutions (Fig. 3). The first one corresponds to the problem of an infinite plate in tension, without the inclusion, which is given in [54] as:

$$u_1^e = \frac{\sigma_0}{2G^e}(1-\nu^e x_1), \qquad u_2^e = -\frac{\sigma_0}{2G^e}(\nu^e x_2), \qquad u_3^e = \phi_3^e = 0. \tag{18}$$

The second solution corresponds to the problem of an inclusion in the infinite domain with displacements/microrotations and stresses/couple stresses vanishing at infinity, while on the boundary of the inclusion

$$\begin{aligned} u_1^e - u_1^i &= f_1 = -\frac{\sigma_0}{2G^e}(1-\nu^e x_1),\\ u_2^e - u_2^i &= f_2 = \frac{\sigma_0}{2G^e}(\nu^e x_2),\\ u_3^e - u_3^i &= f_3 = 0 \end{aligned} \tag{19}$$

and jump in tractions is given as:

$$\begin{aligned} t_1^e - t_1^i &= g_1 = -\sigma_0 n_1,\\ t_2^e - t_2^i &= g_2 = 0,\\ t_3^e - t_3^i &= g_3 = 0. \end{aligned} \tag{20}$$

Therefore, for the boundary element modelling we only consider the circular boundary ∂S^i with inward normal $\vec{n}$ and functions $\boldsymbol{f}$ and $\boldsymbol{g}$ given by Eq. (19) and Eq. (20).

The analytical solution for this problem and the detailed study of the dependence of stress concentration on the material parameters is given in [48] and [49]. The finite element method used as a further verification point was implemented using the DOLFIN [55] finite element library using standard quadratic Lagrangian elements for the displacements and linear Lagrangian elements for the microrotations. We used a graded triangular mesh generated using Gmsh [56]. The code to generate all of the finite element results in this paper, is available at [57]. Note that this standard displacement finite element formulation cannot handle the couple-stress limiting case when $N = 1$ due to a numerical locking effect. To mimic the effect of an infinite domain, we use a mesh with sides of length 20a. We use symmetry boundary conditions so that we only have to model one-quarter of the plate. Here we show the numerical results for 14 cases of the material parameters given in Table 1 and $g = G^i/G^e = 0.5$, $g = 2$. In all cases the remaining material parameters were fixed at $\nu^i = 0.25$, $\nu^e = 1/3$. Note, that case 1 corresponds to the solution for classical elasticity, case 2 represents the inclusion, described by classical elasticity, in a strongly micropolar matrix, case 3 represents a strongly micropolar inclusion in a matrix, described by classical elasticity, case 4 corresponds to equal characteristic lengths, case 5 to equal

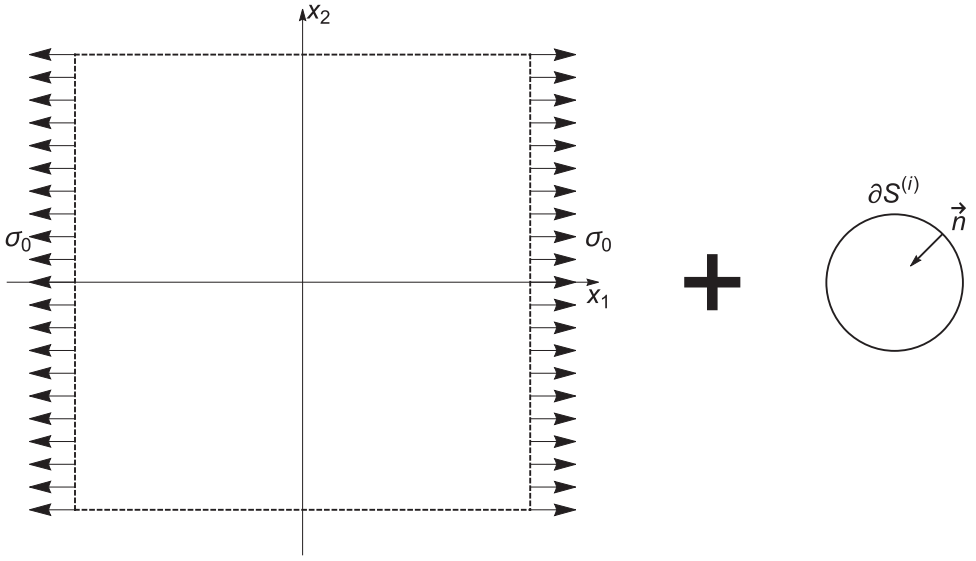

Fig. 3. Superposition of the solutions for the inclusion problem.

Table 1
Material parameters for the study cases in example 1.

	ℓ^i/a	N^i	ℓ^e/a	N^e
1	0.001	0.001	0.001	0.001
2	0.001	0.001	1.000	0.900
3	1.000	0.900	0.001	0.001
4	0.750	0.500	0.750	0.750
5	0.100	0.750	0.750	0.750
6	0.500	0.900	1.000	0.750
7	0.500	1.000	2.000	1.000

Table 2
SCF given by $\sigma^e_{\theta\theta}(\pi/2)$ for $g = 0.5$.

	Analytical solution	BEM	FEM	Error BEM
1	1.57576	1.57540	1.57552	2×10^{-4}
2	1.42722	1.42705	1.42797	1×10^{-4}
3	1.57576	1.57550	1.57551	2×10^{-4}
4	1.46478	1.46455	1.46529	2×10^{-4}
5	1.46707	1.46689	1.46756	1×10^{-4}
6	1.44876	1.44855	1.44926	1×10^{-4}
7	1.35890	1.35871	–	2×10^{-4}

Table 3
SCF given by $\sigma^i_{\theta\theta}(\pi/2)$ for $g = 2$.

	Analytical solution	BEM	FEM	Error BEM
1	1.14872	1.14864	1.14731	7×10^{-5}
2	1.27054	1.27086	1.26864	3×10^{-4}
3	1.14872	1.14890	1.14729	2×10^{-4}
4	1.24128	1.24134	1.23940	5×10^{-5}
5	1.24914	1.24907	1.24673	6×10^{-5}
6	1.26510	1.26486	1.26229	2×10^{-4}
7	1.38507	1.38421	–	6×10^{-4}

couple numbers, case 6 represents a general variation of all material parameters, and case 7 corresponds to the limit case of couple-stress elasticity. In case 7, the results obtained in the present work are in an excellent agreement with the data from [58].

The stress concentration factor (SCF) is defined as

$$\text{SCF} = \max\left\{\frac{\sigma^e_{\theta\theta}(\pi/2)}{\sigma_0}, \frac{\sigma^i_{\theta\theta}(\pi/2)}{\sigma_0}\right\}. \tag{21}$$

The results in terms of the SCFs for all study cases (Table 1) are given in Table 2 for $g = 0.5$ and in Table 3 for $g = 2$, where the excellent agreement between the analytical solution, BEM and FEM results is shown. In all cases, the BEM results were obtained by discretizing the inclusion contour with 36 elements, gradually refined towards the points $\theta = \pm\pi/2$. The FEM results are significantly less accurate than the BEM results, despite the significantly higher number of degrees of freedom required. This finding adds further confirmation to the already well-known superiority of BEM in accurate resolution of stress concentrations around cracks and inclusions in standard elasticity.

4.2. Example 2. Circular inclusion in an infinite domain under remote tension: homogeneously imperfect interface.

As a second example, we consider a problem of a circular inclusion in an infinite plate subjected to a uni-axial tension. The interface between the inclusion and the matrix is assumed to be homogeneously imperfect, i.e. described by Eq. (11) with three interface parameters λ_n, λ_t, λ_ϕ. This problem was studied analytically in [48]. In the present work we demonstrate the application of the boundary element method for the particular cases of the material and interface parameters, i.e. study case 6 of Table 1, for $g = 0.5, 2$ the following values of the interface parameters given in Table 4. The boundary conditions (Eq. (11)) are further superimposed with the solution (Eq. (19) and Eq. (20)) for an infinite plate without a hole, which allows to only consider the inclusion interface as a boundary for the BEM-discretization.

Table 4
Interface parameters for the study cases in example 2.

	$\lambda_n G^e$	$\lambda_\tau G^e$	$\lambda_\phi G^e$
a	0.000	0.000	0.000
b	10.00	10.00	10.00
c	10.00	0.000	0.000
d	0.000	10.00	0.000
e	0.000	0.000	10.00
f	0.000	0.000	1000.

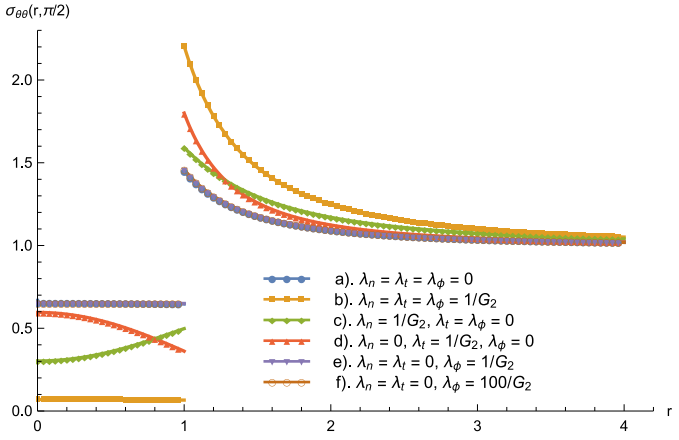

Fig. 4. Distribution of $\sigma_{\theta\theta}(r, \pi/2)$ for $g = 0.5$ for different values of the interface parameters. BEM-data are shown by dots, while the corresponding analytical solutions are given by solid lines.

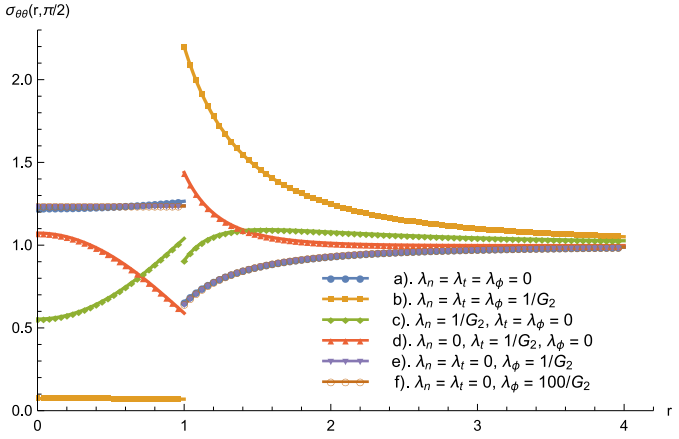

Fig. 5. Distribution of $\sigma_{\theta\theta}(r, \pi/2)$ for $g = 2$ for different values of the interface parameters. BEM-data are shown by dots, while the corresponding analytical solutions are given by solid lines.

The results for both $\sigma^e_{\theta\theta}(\pi/2)/\sigma_0$ and $\sigma^i_{\theta\theta}(\pi/2)/\sigma_0$ are given in Table 5. The results in Table 5 were obtained with 68 elements (612 DOFs) for the discretization of the circle. In all cases a good agreement with the analytical solutions is achieved, with the error within 0.05%.

As it can be observed in Table 5 for $g = 0.5$ the maximum stress at point $\theta = \pi/2$ is always observed in the matrix, while for $g = 2.0$ the maximum stress is observed either in the inclusion, or in the matrix, depending on the values of the interface parameters. Note, that some values of the interface parameters lead to almost no stress concentration (case c) at point $\theta = \pi/2$.

In Figs. 4 and 5 the distribution of $\sigma_{\theta\theta}(r)/\sigma_0$ for various values of the interface parameters is plotted along $\theta = \pi/2$, which demonstrate a good agreement between the BEM-results and the analytical solution. It can be seen, that the stress distribution is much more dependent on the

Table 5
Values of $\sigma^{e}_{\theta\theta}(\pi/2)/\sigma_0$, $\sigma^{i}_{\theta\theta}(\pi/2)/\sigma_0$ for $g = 0.5$, $g = 2.0$ and various values of interface parameters. The numbers in parentheses is the error in comparison with the analytical solution.

a) g = 0.5			b) g = 2		
	$\sigma^{e}_{\theta\theta}(\pi/2)/\sigma_0$	$\sigma^{i}_{\theta\theta}(\pi/2)/\sigma_0$		$\sigma^{e}_{\theta\theta}(\pi/2)/\sigma_0$	$\sigma^{i}_{\theta\theta}(\pi/2)/\sigma_0$
a	1.44898 (0.02 %)	0.64667 (0.009 %)	a	0.65396 (0.003 %)	1.26511 (0.0008 %)
b	2.20480 (0.008 %)	0.06604 (0.01 %)	b	2.19958 (0.002 %)	0.06960 (0.0006 %)
c	1.59208 (0.02 %)	0.49783 (0.008 %)	c	0.90642 (0.01 %)	1.04033 (0.001 %)
d	1.79991 (0.008 %)	0.36191 (0.05 %)	d	1.43881 (0.006 %)	0.58924 (0.01 %)
e	1.45798 (0.02 %)	0.64976 (0.009 %)	e	0.64292 (0.003 %)	1.23772 (0.0008 %)
f	1.45875 (0.02 %)	0.65002 (0.009 %)	f	0.64257 (0.003 %)	1.23685 (< 0.0001 %)

Table 6
SCF given by $\sigma^{(e)}_{\theta\theta}(\pi/2)$ for $g = 0.5$ and various ratios of L/a.

Study cases	$L/a = 1.1$			$L/a = 1.5$Study cases			$L/a = 3.0$		
	BEM	FEM	Δ	BEM	FEM	Δ	BEM	FEM	Δ
1.	1.926	1.923	2×10^{-3}	1.760	1.756	2×10^{-3}	1.680	1.675	3×10^{-3}
2.	2.242	2.240	9×10^{-4}	1.678	1.676	1×10^{-3}	1.478	1.476	1×10^{-3}
3.	2.038	2.036	1×10^{-3}	1.805	1.802	1×10^{-3}	1.683	1.679	2×10^{-3}
4.	2.196	2.214	2×10^{-2}	1.687	1.688	6×10^{-4}	1.522	1.521	7×10^{-4}
5.	2.142	2.140	1×10^{-3}	1.687	1.685	1×10^{-3}	1.526	1.523	2×10^{-3}
6.	2.135	2.132	9×10^{-3}	1.677	1.674	2×10^{-3}	1.502	1.498	3×10^{-3}
7.	2.157	–	–	1.644	–	–	1.410	–	–

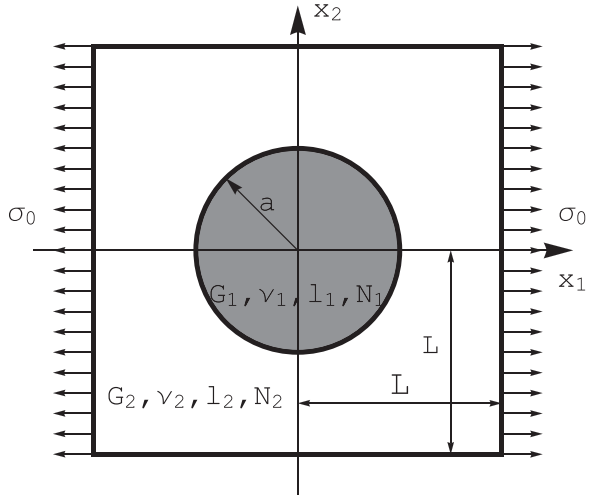

Fig. 6. Circular inclusion in the finite plate.

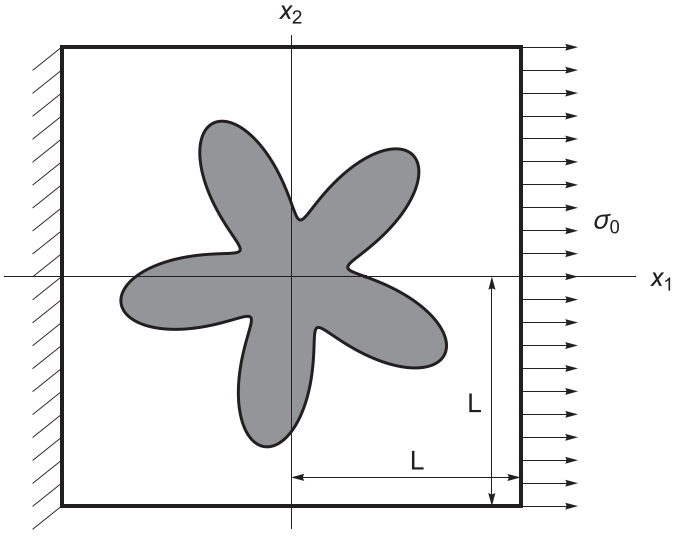

Fig. 7. Inclusion of complex shape.

parameters λ_n and λ_t (cases b, c, d), characterizing bonds in the radial and circumferential directions, than on the parameter λ_ϕ, characterizing jump in the microrotation. The detailed parametric study of this problem is done in [48].

4.3. Example 3. Circular inclusion with perfect interface in a finite plate under uni-axial tension.

In the third example, we consider a circular inclusion with perfect interface in a finite plate of size $2L\times 2L$ subjected to the uniaxial tension, Fig. 6. We consider the same 14 study cases, as in the first example, but this time, we vary the ratio of L/a. The results in terms of the stress concentration factors are shown in Tables 6 and 7 in comparison with the finite element solution [bitbucketlink]. (mesh size, convergence study). The difference between two results is defined as

$$\Delta = \frac{\mathrm{SCF}_{\mathrm{BEM}} - \mathrm{SCF}_{\mathrm{FEM}}}{\mathrm{SCF}_{\mathrm{FEM}}} \tag{22}$$

It's interesting to note, that in the case of $g = 2.0$ and $a/L = 1.1$ no stress concentration occurs for some values of material parameters (cases 2, 4, and 7).

4.4. Example 4. Inclusion of complex shape with perfect interface in a square plate.

In the forth example, we consider an inclusion with perfect interface in a square plate of size $2L\times 2L$ subjected to the boundary conditions (Fig. 7):

$$\begin{aligned} &u_1 = u_2 = \phi = 0 \ \text{ at } \ x = -L, \\ &t_1 = \sigma_0,\ t_2 = t_3 = 0 \ \text{ at } \ x = L. \end{aligned} \tag{23}$$

The size of the plate is set to $L = 2$ mm and the shape of the inclusion is given in the polar coordinates, associated with the point (0, 0) as

$$r(\theta) = 1 + 0.5\sin(5(\theta + \pi/4)) \ \ (\mathrm{mm}). \tag{24}$$

Next, in order to illustrate the influence of the micropolar material constants on the deformation, we compare the numerical results for 8 sets

Table 7
SCF given by $\sigma_{\theta\theta}^{(i)}(\pi/2)$ for $g = 2.0$ and various ratios of L/a.

Study case	$L/a = 1.1$			$L/a = 1.5$			$L/a = 3.0$		
	BEM	FEM	Δ	BEM	FEM	Δ	BEM	FEM	Δ
1.	1.107	1.106	9×10^{-4}	1.149	1.148	9×10^{-4}	1.111	1.111	1×10^{-4}
2.	0.952	0.953	1×10^{-3}	1.138	1.138	1×10^{-4}	1.237	1.236	8×10^{-4}
3.	1.048	1.048	1×10^{-4}	1.089	1.089	1×10^{-4}	1.104	1.104	1×10^{-4}
4.	0.976	0.962	1×10^{-2}	1.144	1.139	4×10^{-3}	1.209	1.203	5×10^{-3}
5.	1.037	1.037	1×10^{-4}	1.166	1.164	2×10^{-3}	1.217	1.216	8×10^{-4}
6.	1.012	1.012	1×10^{-4}	1.160	1.159	9×10^{-4}	1.235	1.234	8×10^{-4}
7.	0.993	–	–	1.178	–	–	1.342	–	–

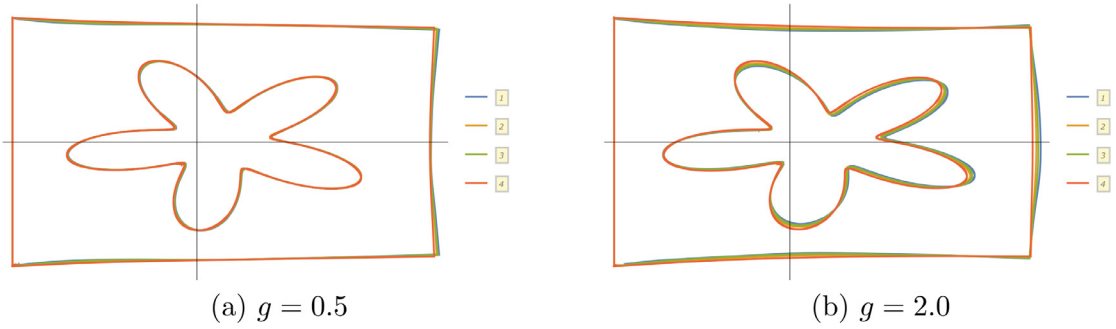

(a) $g = 0.5$ (b) $g = 2.0$

Fig. 8. Deformed contours for study cases (Eq. (25)).

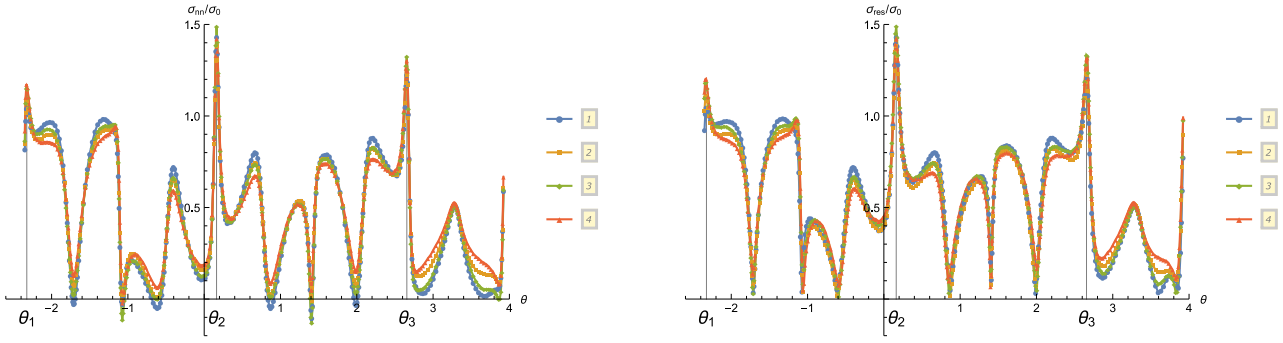

(a) σ_{nn} (b) σ_{res}

Fig. 9. Distribution of the normal and resultant stresses along the inclusion interface for $g = 0.5$ for study cases (Eq. (25)).

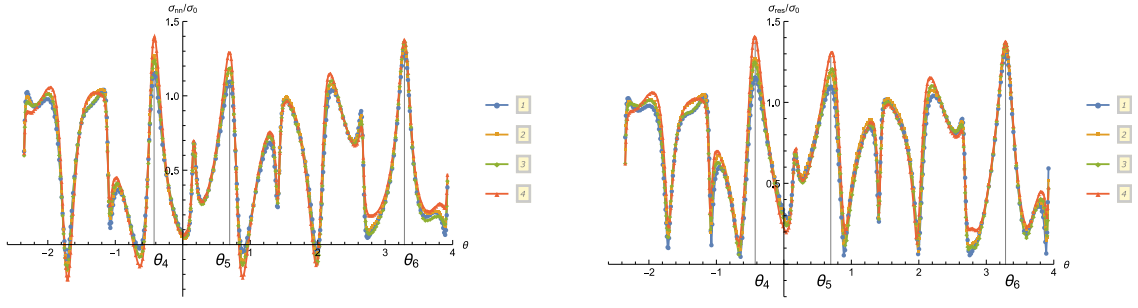

(a) σ_{nn} (b) σ_{res}

Fig. 10. Distribution of the normal and resultant stresses along the inclusion interface for $g = 2.0$ for study cases (Eq. (25)).

of parameters:

1) $\ell^i = 0.001$ mm, $N^i = 0.001$, $\ell^e = 0.001$ mm, $N^e = 0.001$,
2) $\ell^i = 0.1$ mm, $N^i = 0.25$, $\ell^e = 0.5$ mm, $N^e = 0.75$,
3) $\ell^i = 0.9$ mm, $N^i = 0.75$, $\ell^e = 0.1$ mm, $N^e = 0.9$,
4) $\ell^i = 0.5$ mm, $N^i = 1.0$, $\ell^e = 0.75$ mm, $N^e = 1.0$,

(25)

In each case $g = 0.5, 2.0$ and the remaining parameters were fixed to $\nu^i = 0.25$, $\nu^e = 1/3$. First, the (exaggerated) deformed contours are shown in Fig. 8(a), 8(b), where it can be seen that the influence of the chosen micropolar constants on deformation is slightly greater in the case of $g = 0.5$.

Next, the distribution of the normal and resultant stresses defined as

$$\sigma_{nn} = t_1 n_1 + t_2 n_2, \sigma_{res} = (t_1^2 + t_2^2)^{1/2}. \quad (26)$$

along the contour of the inclusion is shown in Fig. 9(a) and 9(b), Fig. 10(a) and10(b), where it can be seen that the micropolar effects on peak stresses (at positions θ_1, ...θ_6) are greater for stiffer inclusions. However, the detailed parametric study of interface failures is a subject of future studies.

5. Conclusion

In this paper the system of boundary integral equations for an inclusion problem in plane micropolar elasticity with imperfect interfaces was formulated and subsequently solved by the boundary element method. The boundary element method is shown to be an efficient tool for numerical analysis of boundary value problems with perfect and imperfect interfaces. For a problem with imperfect interface it is shown that the jump conditions can be directly incorporated into the boundary integral equations.

The results presented in this paper can be further used for analysis of interface failure and crack heterogeneity interaction in Cosserat medium, which is the topic of ongoing work of our team. Another interesting research direction consists in establishing guaranteed homogenization bounds for Cosserat-heterogeneous materials using modern approaches based on stochastic mechanics such as [59].

Supplementary material

FEniCS code to produce the finite element method results can be found at [57].

Acknowledgments

Elena Atroshchenko and Javier Videla are partly supported by Fondecyt Chile, grant No 11130259 entitled "Boundary element modeling of crack propagation in micropolar materials".

Stéphane Bordas thanks funding for his time provided by the European Research Council Starting Independent Research Grant (ERC Stg grant agreement No. 279578) RealTCut Towards real time multiscale simulation of cutting in non-linear materials with applications to surgical simulation and computer guided surgery."

Stéphane Bordas is also grateful for the support of the Fonds National de la Recherche Luxembourg FWO-FNR grant INTER/FWO/15/10318764.

Jack Hale is partly supported by the National Research Fund, Luxembourg, and cofunded under the Marie Curie Actions of the European Commission (FP7-COFUND) Grant No. 6693582.

The authors also acknowledge the support of the Computational Science Research Priority at the University of Luxembourg for visits of Prof. Atroshchenko and to the University of Luxembourg for their support, in particular for access to the High Performance Computing cluster.

References

[1] Al-Rub RKA. Continuum-based modeling of size effects in micro- and nanostructured materials. Pan Stanford Publishing; 2013. 10
[2] Talebi H, Silani M, Bordas SP, Kerfriden P, Rabczuk T. A computational library for multiscale modeling of material failure. Comput Mech 2014;53(5):1047–71.
[3] Mühlhaus EH, Wiley J, Ch N, Lakes R. Continuum models for materials with microstructure. Wiley, Wiley Series in Materials, Modelling and Computation; 1995.
[4] Cosserat E, Cosserat F, Sur la thorie de l'lasticit. Premier mmoire 1896; http://www.numdam.org/item?id=AFST_1896_1_10_3-4_I1_0.
[5] Eringen AC, Linear theory of micropolar elasticity 1965; http://oai.dtic.mil/oai/oai?verb=getRecord&metadataPrefix=html&identifier=AD0473723.
[6] Nowacki W. Theory of asymmetric elasticity. Elsevier Science & Technology; 1986. ISBN 978-0-08-027584-0. Google-Books-ID: yfVQAAAAMAAJ
[7] Eremeyev VA, Lebedev LP, Altenbach H. Foundations of micropolar mechanics. SpringerBriefs in applied sciences and technology. Berlin, Heidelberg: Springer Berlin Heidelberg; 2013. http://link.springer.com/10.1007/978-3-642-28353-6.
[8] Yang JFC, Lakes RS. Experimental study of micropolar and couple stress elasticity in compact bone in bending. J Biomech 1982;15(2):91–8. doi:10.1016/0021-9290(82)90040-9.
[9] Park HC, Lakes RS. Cosserat micromechanics of human bone: strain redistribution by a hydration sensitive constituent. J Biomech 1986;19(5):385–97. doi:10.1016/0021-9290(86)90015-1.
[10] Fatemi J, Keulen FV, Onck PR. Generalized continuum theories: application to stress analysis in bone. Meccanica 37(4–5):385–396. doi:10.1023/A:1020839805384.
[11] Ramzani H, El-Hraiech A, Jeong J, Benhamou C-L. Size effect method application for modeling of human cancellous bone using geometrically exact Cosserat elasticity. Comput Methods Appl Mech Eng 2012;237–240:227–43. doi:10.1016/j.cma.2012.05.002. http://www.sciencedirect.com/science/article/pii/S0045782512001508.
[12] Bigoni D, Drugan WJ. Analytical derivation of Cosserat Moduli via homogenization of heterogeneous elastic materials. J Appl Mech 2006;74(4):741–53. doi:10.1115/1.2711225.
[13] Chen H, Liu X, Hu G, Yuan H. Identification of material parameters of micropolar theory for composites by homogenization method. Comput Mater Sci 2009;46(3):733–7. doi:10.1016/j.commatsci.2009.04.031. http://www.sciencedirect.com/science/article/pii/S0927025609002055
[14] Beveridge AJ, Wheel MA, Nash DH. The micropolar elastic behaviour of model macroscopically heterogeneous materials. Int J Solids Struct 2013;50(1):246–55. doi:10.1016/j.ijsolstr.2012.09.023. http://www.sciencedirect.com/science/article/pii/S0020768312004076
[15] Mühlhaus H-B. Continuum models for layered and blocky rock. In: Analysis and design methods. Elsevier; 1993. p. 209–30. ISBN 978-0-08-040615-2. http://linkinghub.elsevier.com/retrieve/pii/B9780080406152500149
[16] Adhikary DP, Dyskin AV. A Cosserat continuum model for layered materials. Comput Geotech 1997;20(1):15–45. doi:10.1016/S0266-352X(96)00011-0.
[17] Riahi A, Curran JH. Comparison of the Cosserat continuum approach with finite element interface models in a simulation of layered materials. Sci Iran Trans A, Civil Eng 2010;17(1):39. http://search.proquest.com/openview/ef92598e51ee74aac73ce2d513ab4781/1?pq-origsite=gscholar
[18] Onck PR. Cosserat modeling of cellular solids. Comptes Rendus Mcanique 2002;330(11):717–22. doi:10.1016/S1631-0721(02)01529-2.
[19] Tekoglu C, Onck PR. Size effects in the mechanical behavior of cellular materials. J Mater Sci 40(22):5911–5917. doi:10.1007/s10853-005-5042-5.
[20] Duan H, Wang J, Huang Z, Luo Z. Stress concentration tensors of inhomogeneities with interface effects. Mech Mater 2005;37(7):723–36.
[21] Paggi M, Wriggers P. Stiffness and strength of hierarchical polycrystalline materials with imperfect interfaces. J Mech Phys Solids 2012;60(4):557–72.
[22] Zhao X, Bordas SP, Qu J. A hybrid smoothed extended finite element/level set method for modeling equilibrium shapes of nano-inhomogeneities. Comput Mech 2013;52(6):1417–28.
[23] Zhao X, Duddu R, Bordas SP, Qu J. Effects of elastic strain energy and interfacial stress on the equilibrium morphology of misfit particles in heterogeneous solids. J Mech Phys Solids 2013;61(6):1433–45.
[24] Nairn JA. Numerical implementation of imperfect interfaces. Comput Mater Sci 2007;40(4):525–36.
[25] Yvonnet J, Quang HL, He Q-C. An xfem/level set approach to modelling surface/interface effects and to computing the size-dependent effective properties of nanocomposites. Comput Mech 2008;42(1):119–31.
[26] Yvonnet J, He Q-C, Toulemonde C. Numerical modelling of the effective conductivities of composites with arbitrarily shaped inclusions and highly conducting interface. Compos Sci Technol 2008;68(13):2818–25.
[27] Dong H, Wang J, Rubin M. Cosserat interphase models for elasticity with application to the interphase bonding a spherical inclusion to an infinite matrix. Int J Solids Struct 2014;51(2):462–77.
[28] Dong H, Wang J, Rubin M. A nonlinear cosserat interphase model for residual stresses in an inclusion and the interphase that bonds it to an infinite matrix. Int J Solids Struct 2015;62:186–206.
[29] Muskhelishvili NI. Some basic problems of the mathematical theory of elasticity. Dordrecht: Springer Netherlands; 1977. http://link.springer.com/10.1007/978-94-017-3034-1
[30] Mogilevskaya SG, Crouch SL. A Galerkin boundary integral method for multiple circular elastic inclusions with homogeneously imperfect interfaces. Int J Solids Struct 2002;39(18):4723–46. doi:10.1016/S0020-7683(02)00374-8.
[31] Liu YJ, Nishimura N, Otani Y, Takahashi T, Chen XL, Munakata H. A fast boundary element method for the analysis of fiber-reinforced composites based on a rigid-inclusion model. J Appl Mech 2005;72(1):115–28. doi:10.1115/1.1825436.
[32] Huang Q-Z, Xu Z-G, Qiang H-F, Wang G, Zheng X-P. Boundary element method for solid materials with multiple types of inclusions. Acta Mech 2014;226(2):547–70. doi:10.1007/s00707-014-1186-1.
[33] Xue-Hui L, Erdogan F. The crack-inclusion interaction problem. Eng Fract Mech 1986;23(5):821–32.
[34] Natarajan S, Kerfriden P, Mahapatra DR, Bordas SPA. Numerical analysis of the inclusion-crack interaction by the extended finite element method. Int J Comput Methods Eng Sci Mech 2014;15(1):26–32.
[35] Gupta S. An inhomogeneity problem in couple stress theory. In: Proceedings of the indian academy of sciences-section A, 84. Springer; 1976. p. 181–93.
[36] Jasiuk I, Ostoja-Starzewski M. Planar cosserat elasticity of materials with holes and intrusions. Appl Mech Rev 1995;48(11S):S11–18.
[37] Dendievel R, Forest S, Canova G. An estimation of overall properties of heterogeneous cosserat materials. Le J Phys IV 1998;8(PR8):Pr8–111.
[38] Forest S, Dendievel R, Canova GR. Estimating the overall properties of heterogeneous cosserat materials. Model Simul Mater Sci Eng 1999;7(5):829.

[39] Forest S, Pradel F, Sab K. Asymptotic analysis of heterogeneous cosserat media. Int J Solids Struct 2001;38(26):4585–608.
[40] Lubarda V. Circular inclusions in anti-plane strain couple stress elasticity. Int J Solids Struct 2003;40(15):3827–51.
[41] Li L, Xie S. Finite element method for linear micropolar elasticity and numerical study of some scale effects phenomena in MEMS. Int J Mech Sci 2004;46(11):1571–87. doi:10.1016/j.ijmecsci.2004.10.004. http://www.sciencedirect.com/science/article/pii/S0020740304002590
[42] Jeong J, Ramzani H, Mnch I, Neff P. A numerical study for linear isotropic Cosserat elasticity with conformally invariant curvature. ZAMM - J Appl Math Mech / Z Angew Math Mech 2009;89(7):552–69. doi:10.1002/zamm.200800218.
[43] Bauer S, Schfer M, Grammenoudis P, Tsakmakis C. Three-dimensional finite elements for large deformation micropolar elasticity. Comput Methods Appl Mech Eng 2010;199(4144):2643–54. doi:10.1016/j.cma.2010.05.002. http://www.sciencedirect.com/science/article/pii/S0045782510001441
[44] Natarajan S, Chakraborty S, Thangavel M, Bordas S, Rabczuk T. Size-dependent free flexural vibration behavior of functionally graded nanoplates. Comput Mater Sci 2012;65:74–80. arXiv: 1203.36439
[45] Natarajan S. On the application of the partition of unity method for nonlocal response of low-dimensional structures. J Mech Behav Mater 2014;23(5–6):153–68.
[46] Atroshchenko E, Bordas SPA. Fundamental solutions and dual boundary element methods for fracture in plane Cosserat elasticity. Proc R Soc A 2015;471(2179). doi:10.1098/rspa.2015.0216.
[47] Hadjesfandiari AR, Dargush GF. Boundary element formulation for plane problems in couple stress elasticity. Int J Numer Methods Eng 2012;89(5):618–36. doi:10.1002/nme.3256.
[48] Videla J, Atroshchenko E. Analytical study of a circular inhomogeneity with homogeneously imperfect interface in plane micropolar elasticity. ZAMM - J Appl Math Mech / Z Angew Math Mech 2017. doi:10.13140/RG.2.1.1689.5846. In Press
[49] Videla J, Atroshchenko E. Analytical study of a circular inhomogeneity with homogeneously imperfect interface in plane micropolar elasticity. Supporting material. https://sourceforge.net/projects/micropolarinclusion/.
[50] Schiavone P.. Integral equation methods in plane asymmetric elasticity. J Elast 43(1):31–43. http://link.springer.com/article/10.1007/BF00042453. doi:10.1007/BF00042453.
[51] Iean D. Existence theorems in the theory of micropolar elasticity. Int J Eng Sci 1970;8(9):777–91. doi:10.1016/0020-7225(70)90004-2.
[52] Atroshchenko E, Bordas SPA. Fundamental solutions and dual boundary element methods for fracture in plane Cosserat elasticity. https://sourceforge.net/projects/cosseratfundamentalsolutions/.
[53] Telles JCF, Oliveira RF. Third degree polynomial transformation for boundary element integrals: further improvements. Eng Anal Bound Elements 1994;13(2):135–41. doi:10.1016/0955-7997(94)90016-7.
[54] Paul HS, Sridharan K. The problem of a griffith crack in micropolar elasticity. Int J Eng Sci 1981;19(4):563–79. doi:10.1016/0020-7225(81)90090-2.
[55] Logg A, Wells GN. DOLFIN: automated finite element computing. ACM Trans Math Softw 2010;37(2) 20:1–20:28. doi:1145/1731022.1731030.
[56] Geuzaine C, Remacle J-F. Gmsh: A 3-D finite element mesh generator with built-in pre- and post-processing facilities. Int J Numer Methods Eng 2009;79(11):1309–31. doi:10.1002/nme.2579.
[57] Atroshchenko E, Hale JS, Videla J, Potapenko S, Bordas SPA. Microstructured materials: inhomogeneities and imperfect interfaces in plane micropolar elasticity, a boundary element approach. Supporting material https://dx.doi.org/10.6084/m9.figshare.4047462. 10.6084/m9.figshare.4047462.
[58] Weitsman Y. Couple-stress effects on stress concentration around a cylindrical inclusion in a field of uniaxial tension. J Appl Mech 1965;32(2):424–8. doi:10.1115/1.3625817.
[59] Paladim D-A, de Almeida JPB, Bordas S, Kerfriden P. Guaranteed error bounds in homogenisation: an optimum stochastic approach to preserve the numerical separation of scales; 2017. IJNME (accepted for publication).